

Particles and Fields in Radio Galaxies
ASP Conference Series, Vol. , 2001
Robert A. Laing and Katherine M. Blundell

Nonthermal Emission in Radio Galaxies from Simulated Relativistic Electron Transport in 3D MHD Flows

I. L. Tregillis, T. W. Jones

School of Physics and Astronomy, University of Minnesota, 116 Church St. S.E., Minneapolis, MN 55455, USA

Dongsu Ryu

Department of Astronomy and Space Science, Chungnam National University, Daejon, 305-764, Korea

Abstract. We perform a series of so-called “synthetic observations” on a set of 3D MHD jet simulations which explicitly include energy-dependent transport of relativistic electrons, as described in the companion paper by Jones, Tregillis, & Ryu. Analyzing them in light of the complex source dynamics and energetic particle distributions described in that paper, we find that the standard model for radiative aging in radio galaxies does not always adequately reflect the detailed source structure.

1. Introduction

Jones, Ryu, & Engel (1999) presented the first multidimensional MHD simulations to include explicitly time-dependent transport of the relativistic electrons responsible for the nonthermal emission observed from extragalactic radio sources. The companion paper by Jones, Tregillis, & Ryu (2000; paper I) in this proceedings describes results from the extension of that work to three dimensions via exploratory simulations designed to probe the relationships between the source dynamics and the spatial and energy distributions of nonthermal electrons.

We compute self-consistent emission properties for the simulated sources, thereby producing the first “synthetic observations” of their kind, including synchrotron surface brightness and spectral index maps. This paper briefly summarizes some of these synthetic observations. A full report is in preparation.

2. Synthetic Observation Methods

In every zone of the computational grid we compute an approximate, self-consistent synchrotron emissivity as described in Jones et al. (1999). This calculation is performed in the rest frame of the simulated radio galaxy, with the appropriate redshift correction made for the observation frame. It also explicitly takes into account the three-dimensional magnetic field geometry. Note that because we are explicitly calculating the momentum distribution of nonthermal electrons, we obtain the local synchrotron spectral index α directly.

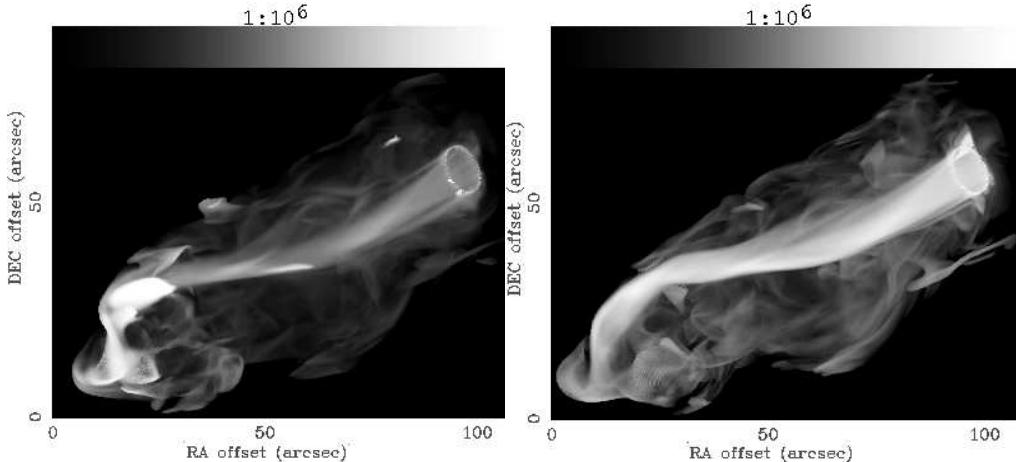


Figure 1. 1.4 GHz synchrotron surface brightness maps. The “injection” model is on the left and “strong-cooling” on the right.

Previously, spectral indices in synthetic observations from purely MHD simulations had to be included in an ad hoc fashion (Matthews & Scheuer 1990; Clarke 1993).

Surface brightness maps for the optically thin emission are then produced via raytracing through the computational grid to perform line-of-sight integrations, thereby projecting the source on the plane of the sky at any arbitrary orientation. The synthetic observations can be imported into any standard image analysis package and subsequently analyzed like real observations; the analysis here was performed using the MIRIAD and KARMA (Gooch 1995) packages. For example, it is a straightforward matter to construct spectral-index maps from a set of observations over a range of frequencies. To make this exercise as realistic as possible we place the simulated object at an appropriate luminosity distance, set to 100 Mpc for the observations included here. Because our primary interest here is in identifying general trends, the observations are presented at their full resolution with very high dynamic range, although it is straightforward to convolve the images down to lower resolution before making comparisons to true observations.

3. Discussion

The dynamical effects outlined in the paper I have a profound impact on the nonthermal electron populations in these simulated sources. For the purpose of contrasting two extreme cases, here we will consider only the “injection” and “strong-cooling” electron-transport models (models 2 and 3 in paper I).

Figure 1 shows synthetic synchrotron surface brightness maps computed at 1.4 GHz, corresponding to a time when the jet has propagated about 30 jet radii. Consider first the “injection” transport model. A jet, hotspot complex, and lobe are all readily visible. The bright ring in the upper right is the orifice where the jet enters the computational grid.

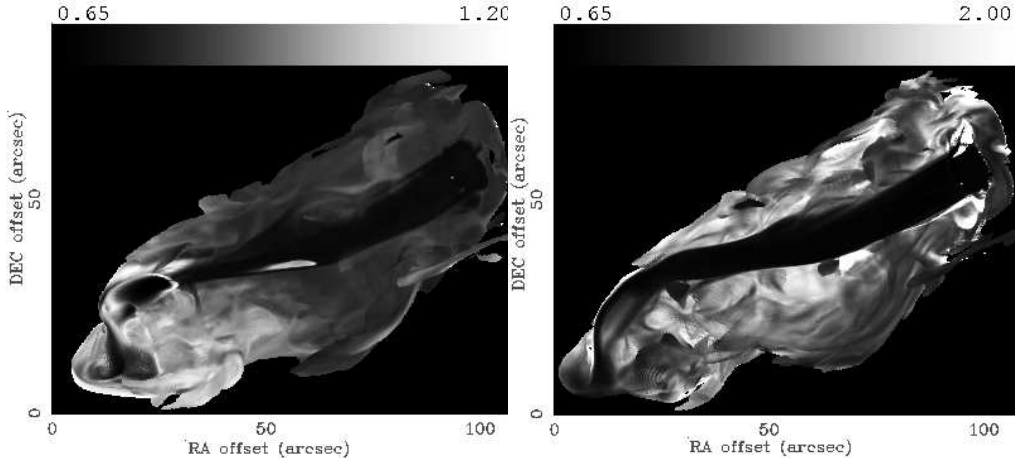


Figure 2. Two-frequency spectral index maps computed from surface brightness at 1.4 and 5.2 GHz. The “injection” model is on the left and “strong-cooling” on the right.

The apparent hotspot complex consists of a bright, compact primary hotspot and a weaker, more diffuse secondary hotspot slightly below it. This secondary hotspot is a “splatter spot” (Cox, Gull, & Scheuer 1991; Lonsdale & Barthel 1986); we also see “dentist’s drill” type hotspots (Scheuer 1982) at other times.

In the case shown here, the bright primary hotspot does correspond to a strong shock at the jet terminus, although this is often not the case. The synchrotron emissivity jumps by a factor of nearly 10^4 across this shock in the injection model because the model assumes almost no relativistic electrons enter with the jet flow. Rather, they are supplied through shock injection. The magnetic pressure increases by merely a factor of 2.5. Thus, we have an example of a prominent hotspot where the brightness is primarily the result of enhanced particle populations rather than dramatic magnetic field growth.

Contrast this with the situation in the “strong cooling” transport model. There, the jet core dominates the emission, because the entire nonthermal particle population enters the grid with the jet. Although there is a minor brightness enhancement, we no longer see such a dramatic hotspot at the location of the terminal shock, despite the fact that these two models are dynamically identical. Virtually all of the brightness variations in this model are signaling variations in the underlying magnetic field structure.

These models also give rise to fascinating spectral index maps. Figure 2 shows two-frequency spectral index maps computed from surface brightness maps at 1.4 and 5.2 GHz. Once again considering the injection model first, we see that the jet, hotspot, and lobe are easily identifiable. The jet has a synchrotron spectral index of 0.7, consistent with the momentum index of 4.4 for the particles sent down the jet. The primary hotspot is slightly flatter than this, in accordance with the presence of a strong shock. The lobe spectrum is somewhat peculiar, however, with material in the head region steeper than that towards the core; this is quite the opposite from what would be expected based on the standard paradigm for radio galaxy aging. This surprising result is an excellent

example of the impact of the shock-web complex described in paper I. Injection at the numerous weak shocks spread throughout the head region increases the steep-spectrum particle populations enough that they can temporarily dominate the emission, a task made easier by the relatively small flatter population sent down the jet in this model. The lobe emission becomes less steep as the two populations begin to mix in the backflow, since radiative losses are minimal here. Since injection acts to create convex spectra, the emission is flattened even further as the emitting particles diffuse into the large low-field volumes in the cocoon.

The complicated spectral index map from the strong cooling model vividly demonstrates the extreme variability of the magnetic field in these sources. Strong fluctuations in the field make it possible to create distinct regions within the same source between which the effective cooling rate differs by orders of magnitude. Also, these sources are rather young in terms of their histories, so individual events in the source evolution can still have a discernible effect upon the overall appearance at these times. For instance, the region of moderately-steep material located below the jet midway along the cocoon can be traced to a particular instance where shearing flows generated at the jet tip lead to a dramatic but transient enhancement of the local magnetic field.

This work is supported by the U. S. National Science Foundation and the University of Minnesota Supercomputing Institute, and in Korea by KOSEF.

References

Clarke, D. A. 1993, ‘3-D MHD simulations of extragalactic jets’ in Lecture Notes in Physics Vol. 421, Jets in Extragalactic Radio Sources, ed. H.-J. Röser & K. Meisenheimer (Berlin: Springer), 243–252

Cox, C. I., Gull, S. F., & Scheuer, P. A. G. 1991, ‘Three-dimensional simulations of the jets of extragalactic radio sources’, MNRAS, 252, 558–585

Gooch, R. E. 1995, ‘Karma: a visualisation test-bed’ in ASP Conf. Ser. Vol. 152, Astronomical Data Analysis Software and Systems V, ed. G. H. Jacoby & J. Barnes, (San Francisco: ASP), 80–83

Jones, T. W., Tregillis, I. L., Ryu, Dongsu 2001, ‘3D MHD simulations of relativistic electron acceleration and transport in radio galaxies’, these proceedings (paper I)

Jones, T. W., Ryu, Dongsu, & Engel, Andrew 1999, ‘Simulating electron transport and synchrotron emission in radio galaxies: shock acceleration and synchrotron aging in axisymmetric flows’, ApJ, 512, 105–124

Lonsdale, C. J., & Barthel, P. D. 1986, ‘Double hotspots and flow redirection in the lobes of powerful extragalactic radio sources’, AJ, 92, 12–22

Matthews, A. P., & Scheuer, P. A. G. 1990, ‘Models of radio galaxies with tangled magnetic fields - I. calculation of magnetic field transport, Stokes parameters and synchrotron losses’, MNRAS, 242, 616–622

Scheuer, P. A. G. 1982, ‘Morphology and power of radio sources’, in IAU Symp. 97, Extragalactic Radio Sources, ed. D. S. Heeschen & C. M. Wade (Dordrecht: Reidel), 163–165